

Efficient Multiparty Entanglement Distribution with DODAG-X Protocol

Roberto Negrin¹, Nicolas Dirneger², William Munizzi¹,
Jugal Talukdar¹, Prineha Narang^{1,2}

¹*Division of Physical Sciences, College of Letters and Science, University of California, Los Angeles*

²*Electrical and Computer Engineering Department, University of California, Los Angeles*

Email: wmunizzi17@ucla.edu, prineha@ucla.edu

August 15, 2024

Abstract

In this work we introduce the DODAG-X protocol for multipartite entanglement distribution in quantum networks. Leveraging the power of Destination Oriented Directed Acyclic Graphs (DODAGs), our protocol optimizes resource consumption and enhances robustness to noise in dynamic and lossy networks. Implementing a variation on the X-protocol within the DODAG, we minimize graph verification and path-finding calculations, significantly reducing computational overhead when compared to other entanglement routing schemes. Additionally, our benchmarks on grid lattice and small-world topologies reveal substantial measurement reduction compared to existing protocols. We demonstrate the success of DODAG-X for generating maximal three-party entanglement in arbitrary networks, and describe the potential for scaling to generic n -party entanglement. The DODAG-X protocol provides a scalable and efficient solution for entanglement routing, advancing current techniques for reliable quantum communication and network applications.

Contents

1	Introduction	3
1.1	Background	3
1.2	Previous Work	3
1.3	Our Contribution	4
2	Review	6
2.1	Graph Theory	6
2.2	Graph States	7
2.3	X-protocol	8
2.4	Dynamic Network	9
2.5	DODAG Structure	10
3	DODAG-X Protocol	11
3.1	The Protocol	11
3.2	Complexity in DODAG-X	14
3.3	Generalizations to Higher Party Number	15
4	Performance Benchmarks	17
4.1	Grid Lattice Networks	17
4.2	Small-World Networks	19
5	Discussion and Future Work	21
6	Acknowledgements	22
A	Path-Finding Complexity	27
B	Proofs of Connectivity	27
B.1	Proofs of Entangled Intersections	27
B.2	Proof of Entangled Pairs	29
B.3	Proof of Isolated Entangled Triplets	29
C	Measurement Counts	30
C.1	Path Measurements	30
C.2	Isolation Measurements	32
D	Additional Performance Benchmarks	32

1 Introduction

1.1 Background

Quantum networks play an important role in the ongoing development of distributed quantum computation, particularly in the creation of modular quantum computing systems and secure communication protocols for quantum key distribution [1, 2]. Notoriously, however, quantum systems are extremely noisy, leaving underlying network protocols, e.g. long-distance entanglement generation, prone to loss and error [3, 4]. Noise issues in quantum systems arise from a variety of factors including, but not limited to, environmental interference, imperfect quantum channels, qubit thermalization, and current (or even fundamental) technological limitations [5, 6]. To this end, numerous protocols have been developed to perform critical routing tasks, such as entanglement swapping or measurement-based entanglement distribution [7, 8, 9]. Each protocol typically incorporates a combination of quantum and classical techniques to overcome technological limitations, working towards the common goal of establishing high-fidelity entanglement over long-distance channels.

While entanglement generation between two parties has been studied extensively in previous years [10], efficient techniques for multipartite entanglement distribution remain elusive. The impending need for n -party entanglement manipulation in quantum networks necessitates new ideas and tools for analyzing network properties. One such tool uses graph states to represent quantum networks, and employs graph-theoretic techniques to explore entanglement evolution in the representative state [11]. Graph states are multipartite entangled states, defined using a mathematical graph, where each vertex represents a qubit and each edge a correlation, e.g. entanglement, between qubits [12]. Given the utility for graph states to represent multipartite entanglement, they arise throughout many quantum information processing domains including measurement-based quantum computing [13], quantum error-correction [14], quantum secret sharing [15], and quantum metrology [16].

When using graph states to describe entanglement in quantum networks, we rely on the notion of constructible entanglement between different network nodes. We distinguish between graphs representing the physical network, with qubits as nodes and communication channels, e.g. optical fibers, as edges, and the graph representing the virtual topology (sometimes called the “instant topology”), in which edges define the entanglement between qubit nodes [17]. In this context, entanglement distribution refers to a manipulation of nodes in the physical network to obtain a desired graph structure in the virtual topology. The challenge then becomes: how best to arrange and modify the quantum network, and how to optimize routing protocols over its graph connectivity, to efficiently construct the desired entanglement.

1.2 Previous Work

Many previous works have explored multipartite entanglement in quantum networks, using a graph state representation, such as [18, 19] which focused on three and four qubit GHZ state construction. In [19] an extension was developed for building GHZ_n , using min-

imal assumptions about the underlying structure of the network. Each protocol utilizes entanglement routing, based in local measurement, to create end-to-end entanglement between distant nodes in the quantum network. Both schemes, while foundational in their advancement of entanglement routing techniques, are subject to resource constraint and exhibit unfavorable complexity scaling for large networks.

In [18] the authors introduce the X-protocol for entangling any two nodes in a quantum network, using only local measurements, without the need for initially isolating the subsystem of interest. The X-protocol is performed in contrast to the standard repeater protocol, in which the shortest path connecting the two nodes in the quantum network is selected and isolated prior to measurement. As mentioned prior, the X-protocol enables efficient entanglement generation between multiple parties, up to four, and can be extended with additional resources to n parties [19]. However, constructing n -party GHZ states requires the graph possess a repeater line in the form of a vertex minor, which hinders success for certain graph configurations. Furthermore, the X-protocol requires a path-finding algorithm to be performed prior to entangling each pair of parties. While repeated path searches may be feasible for small graphs, for larger networks (or highly-connected networks) the process rapidly becomes intractable. The problem of optimal path-finding in generic graphs is difficult, and even NP hard in certain cases which apply to quantum networks, and is often addressed using well-known algorithms such as Dijkstra, Breadth-First-Scan (BFS), or Bellman-Ford, among others.

Further works have focused on graph state generation, in addition to entanglement routing algorithms, in quantum networks with certain assumptions [20, 21, 22]. This parallel approach exploits the stochastic nature of quantum operations and subgraph complementation to optimally compose graph states in particular networks. In [21], for example, two optimized schemes for generating tree graph states are derived using linear programming, subject to resource and fidelity constraints. We acknowledge the novelty and utility of these techniques, but our work will focus on improving entanglement routing schemes.

In [17] a routing technique is proposed that uses a Destination Oriented Directed Acyclic Graph (DODAG) to maintain entanglement in the virtual topology, despite connection loss in the physical network. While DODAGs have long occupied a prominent role in classical communication, allowing multiple users to transmit information simultaneously in a dynamic network [23], their extension to quantum networks remains largely unexplored. The authors of [17] compose a set of asynchronous routing protocols for pairwise entanglement, in contrast to entanglement swapping using synchronized time slots, achieving significantly higher entangling rates than existing schemes. We will expand on this idea of multipartite entanglement routing, combining a DODAG tree structure with merge-based methods for improved measurement and complexity performance.

1.3 Our Contribution

In this work, we combine a measurement-based procedure for routing entanglement, with a semi-classical DODAG to preserve the entanglement structure in time [17]. Our approach is optimized for a virtual network with tree topology, set by the DODAG, which can be faithfully maintained even in realistic and lossy networks. We prove that this protocol can produce arbitrary entanglement for up to three parties in any quantum net-

work, as well as generic n -party entanglement in networks with certain structure. We benchmark the performance of our protocol, with regards to resource consumption and computational complexity, against existing entanglement routing schemes.

In the above context, we make the following contributions:

- **Improved Resource Efficiency:** We develop a method that optimizes resource consumption, particularly focusing on the number of quantum measurements required to complete the entanglement protocol. This reduction in resources is critical for implementation in large-scale networks, where resources are often limited.
- **Improved Complexity Scaling:** We utilize a tree structure to minimize path-finding complexity between parties. This construction offers significant improvements over traditional models, which incorporate numerous and costly path-finding steps throughout the entangling protocol.
- **Integration of DODAG with Entanglement Routing:** We maintain robustness to noise, even in the presence of dynamic and lossy physical networks, by pairing our entanglement routing scheme with a DODAG to preserve the entanglement structure in time.
- **Scalable GHZ State Formation:** We introduce a protocol that supports GHZ generation for up to three, and often more, parties. We demonstrate the efficient scaling of our method, a critical aspect for realizing larger quantum networks.
- **Performance Benchmarks:** We benchmark the performance of our protocol, alongside the X-protocol, for candidate quantum network topologies of different sizes. We account for all measurements needed to complete both protocols, as well as the complexity of classical path-finding processes employed throughout the entangling procedure.

The remainder of the paper is organized as follows. In Section 2 we review necessary theory on graphs and graph states, the notion of dynamic networks and DODAGs, and the details of the X-protocol routing scheme. In Section 3 we introduce the DODAG-X protocol and analyze its complexity for different quantum networks. We demonstrate generalizations of DODAG-X for higher party entanglement routing, and propose near-term realizable extensions concatenated networks. We directly benchmark the performance of DODAG-X, along with the X-protocol, in Section 4. We compare the average number of measurements needed to complete each protocol, for entangling all possible party triplets, in networks with grid lattice and Small-World topologies. In Section 5 we conclude and discuss future directions for this work. An Appendix collections necessary proofs, as well as additional performance benchmarks.

2 Review

2.1 Graph Theory

A graph $G = (V, E)$ is defined as a set of vertices V , and a set of edges E . Every edge $e \in E$ can be described as an ordered pair $\{u, v\}$, with $u, v \in V$ the vertices connected by e , and thereby $E \subseteq V \times V$. In an undirected graph, edges are not oriented, and consequently $\{u, v\} = \{v, u\}$. Removing an edge $e \in E$ from G results in a new graph

$$\bar{G} \equiv G \setminus e = (V, E \setminus \{e\}). \quad (1)$$

Likewise, the process of removing a vertex from G generates the graph

$$\bar{G} \equiv G - v = G(V \setminus \{v\}, \{(i, j) \in E : i, j \neq v\}). \quad (2)$$

In the context of graphs representing quantum systems, the operations in Eqs. (1) and (2) correspond to measurements performed on the physical system. We discuss these measurements in more detail shortly.

A graph path $P_{0,k}$ is a sequence of distinct vertices $\{v_0, v_1, \dots, v_k\}$, such that each pair of adjacent vertices $\{v_i, v_{i+1}\}$ is an element of the edge set E . Similarly, the neighborhood N_v of a vertex $v \in V$ is defined

$$N_v = \{u \in V | (u, v) \in E\}, \quad (3)$$

and describes the set of all vertices that share an edge with v . We emphasize that the neighborhood N_v never contains vertex v as an element.

The *local complementation* operation on a graph G , at a vertex $v \in V$, results in a new graph $\bar{G} \equiv LC_v(G)$, where the subgraph of G generated by N_v is replaced by its graph complement. In other words, all edges connecting N_v in G are removed in \bar{G} , and all vertices in N_v that were disconnected in G are now connected in \bar{G} . Formally, the process of local complementation can be defined as

$$LC_v(G) = \bar{G} = (V, E \Delta \{(i, j) | i, j \in N_v, i \neq j\}), \quad (4)$$

where Δ denotes the symmetric difference [24]. Figure 1 depicts an example of local complementation, and the associated graph transformation.

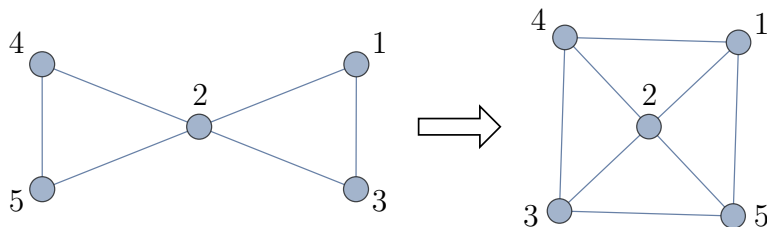


Figure 1: The process of local complementation, on vertex 2 of the left graph, is depicted above. The result is a new graph where the subgraph generated by the neighborhood N_2 has been replaced with its complement.

In the context of quantum networks, graphs are used to describe and analyze correlated quantum systems. Vertices, typically referred to as “nodes” in network theory, represent qubits (or systems of qubits) which are connected via communication channels (edges in the graph). In the upcoming sections we extrapolate this graph formalism for quantum networks, detailing how the above graph transformations can be implemented by measurement, resulting in entanglement distribution across the network.

2.2 Graph States

When working with quantum networks, we are interested in understanding both the global structure of the physical network, as well as the interactions between constituent nodes. Most importantly for any quantum application, we are interested in understanding the entanglement structure in a quantum network, and how entanglement can be distributed over desired nodes with sufficient fidelity. One useful tool for modeling a quantum network, as well as the entanglement structure therein, is a *graph state*.

A graph state $|G\rangle$ is a quantum state which admits a graph representation, where vertices represent qubits and edges represent non-local interactions between those qubits [11]. In this way, each graph state describes the “entanglement history” of the qubits that comprise it. Since we are interested in qubits which share an EPR type entanglement, we can precisely define a graph state $|G\rangle$ as

$$|G\rangle := \bigotimes_{(u,v) \in E} CZ_{u,v} |+\rangle^{\otimes |V|}, \quad (5)$$

where each qubit, corresponding to a vertex $v \in V$, is initialized in the state $|+\rangle = (|0\rangle + |1\rangle)/\sqrt{2}$. Entanglement in Eq. (5) is generated by the Controlled-Z gate, denoted $CZ_{u,v}$, where u indicates the control qubit and v the target qubit. The $CZ_{u,v}$ is a two qubit operation that initiates a Pauli Z operation on the target qubit iff the control qubit is “on”. While this definition for graph states is useful in practice, physical preparation of a generic graph state is not restricted to this specific method [25, 26].

Two graphs G and G' , representing states $|G\rangle$ and $|G'\rangle$, are locally equivalent if $|G\rangle$ and $|G'\rangle$ are equal up to some local unitary (LU) operation [11]. In other words, we say that G and G' are *LU-equivalent* if there exists a local unitary U such that

$$|G'\rangle = U |G\rangle. \quad (6)$$

For graph states defined as in Eq. (5), local Clifford operations (any unitary generated by Hadamard and phase gates) always generate graphs that are LU-equivalent to G [27].

The process of performing a local Pauli measurement on a graph state generates a transformation on the associated graph [18]. Given a multiqubit graph state $|G\rangle$, the effect of performing a Pauli-Z measurement on the qubit denoted by vertex v corresponds to removing that vertex from the graph,

$$Z_v(G) = G - v. \quad (7)$$

Similarly, performing a Pauli-X measurement on qubit v in $|G\rangle$ generates a series of local complementations, and a single Z measurement, on G . Specifically,

$$X_v(G) = LC_w Z_v LC_v LC_w(G), \quad (8)$$

where w is some chosen vertex in N_v . To simplify the notation in Eqs. (7) and (8), we write Z-measurements as $Z[v]$ and X-measurements as $X[v, w]$ going forward. It is important to note that, depending on the choice of w , an X measurement can generate several different graphs. However, any graph obtained via $X[v, w]$ is LU-equivalent to any other [28, 29]. We specify the chosen neighbor w when it is useful for understanding the resultant graph.

When performing repeated measurements on a graph state, it quickly becomes useful to introduce a notation describing the corresponding graph evolution after each operation is applied. We define the object $N_v^{(n)}$ to be the neighborhood of v after n Pauli measurements have occurred. In most cases we need only consider the effect of X-measurements, but will specify each operation nonetheless. In other contexts it can be convenient to adopt the related notation $N_v^{(u)}$, which indicates the neighborhood of v after a measurement is performed on the vertex u . We make sure to clarify which neighborhood notation is in use, whenever it may be otherwise ambiguous.

Since graph states capture the entanglement structure shared among a system of qubits, they offer a natural model for entanglement distribution in quantum networks. More directly, since entanglement manipulation in graph states can be described through a sequence of operations on an initial state, sequential measurements on a given graph state can yield a mechanism for routing entanglement in a quantum network isomorphic to the associated graph. When implementing this prescription, both the number of measurements and the specific vertices being measured determine the entanglement structure in the final graph state. In the following section, we detail one successful protocol for entanglement routing among three parties, known as the X-protocol.

2.3 X-protocol

In this section we outline the entanglement routing X-protocol, presented by Hahn, Pappa, and Eisert in [18]. The X-protocol was conceived to distribute entanglement between 2 parties in a quantum network, but can be applied to entangle 3 parties as well. In [19] the X-protocol was extended to generate n -party entanglement, under certain restrictions. We summarize the protocol below for entangling 2 arbitrary nodes in a network, and illustrate the procedure in Figure 2.

1. Identify the shortest path between two nodes of interest, denoted as a and b . Normally, this process is performed using an algorithm such as Dijkstra.
2. Next perform an X measurement on each node along this shortest path, excluding measurement on a and b themselves.
3. After all X measurements have been applied, perform a Z measurement on all nodes in the neighborhoods N_a and N_b , again excluding nodes a and b .

After completing Steps 1–3 above, nodes a and b will exist in an EPR state. As a result, entanglement has been effectively routed through the quantum network using only local qubit measurements. The process for applying the above to entangle 3 qubits follows a similar procedure, and is likewise presented in [18]. Figure 2 illustrates the X-protocol performed to entangle three parties in a 16-node grid network.

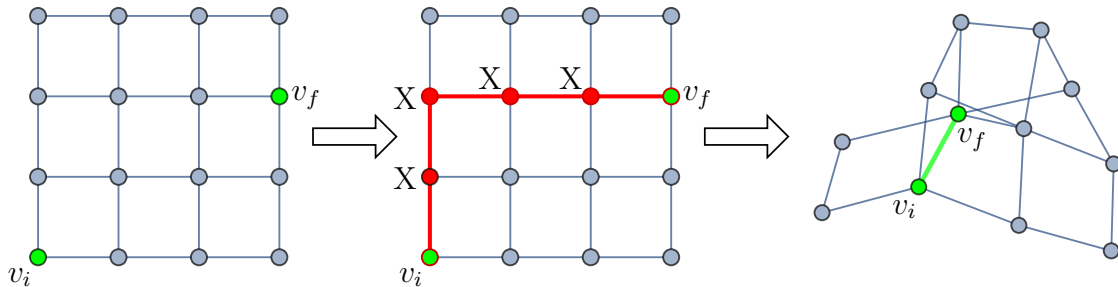


Figure 2: The X-protocol first selects 2 nodes to entangle, v_i and v_f , shown in green. The shortest path between v_i and v_f is computed, in red. Each node along this path is X-measured, using v_i for local complementation. The result is v_i and v_f in an EPR state.

To generalize the X-protocol to n parties, we require that the underlying quantum network satisfies a vertex minor condition, specifically that successive applications of local complementation and vertex deletion can always distill a subgraph from the initial graph. Furthermore, the shortest path between two nodes must contain an additional node inserted between each pair of $n - 2$ intermediate nodes. Following the X-protocol, along with these conditions, yields an n -party GHZ state again using only local operations. Reliably finding the shortest paths between n nodes in an arbitrary graph, Step 1 above, is a non-trivial process. Well known algorithms such as Dijkstra admit scaling performance as bad as $\mathcal{O}(|E| + n \log(n))$.

In both [18] and [19] the authors focus on static networks, where the graph structure is constant in time. Unfortunately, realistic quantum networks are expected to be highly variable in time due to decoherence, thermalization, and additional environmental factors. This crucial factor necessitates the need for a protocol which can be applied successfully on dynamic networks with variable topology. In the following sections we discuss dynamic networks in detail, and introduce techniques for handling their inherent variability.

2.4 Dynamic Network

Before exploring the properties of dynamic networks, it is important to first understand the structural difference between static and dynamic networks. In a static network all communication channels are operational at all times, which enables classical offline pre-processing. Conversely, in a dynamic network the set of operational channels is a function of time, meaning connections may fail and recover arbitrarily. It is assumed that nodes in the network know the status of their incident links at all times.

A realistic quantum network is a dynamic network, meaning the topology of the network changes over time mainly due to decoherence [30], when connections between nodes may be lost. For this reason it is necessary to differentiate between the physical topology and the virtual topology, sometimes referred to as the instant topology [17]. The physical topology describes the hardware connection between nodes in the network. This connection can be established using, for example, optical fibers. The virtual topology refers to the entanglement structure between nodes in the network, which do not necessarily have any direct communication channel through hardware. Figure 3 illustrates the embedding of a virtual topology into the physical network.

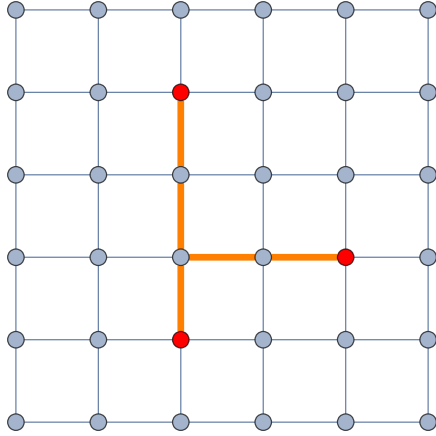


Figure 3: Physical network with lattice topology, consisting of 36 nodes. Gray edges represent hardware communication channels between nodes, e.g. optical fibers. The virtual topology is highlighted in orange, where the red nodes exist in an entangled state.

When constructing the virtual topology, i.e. entangling nodes in a network, some form of routing protocol must be implemented. An effective quantum routing protocol must identify optimal paths when required, as well as determine alternative paths if a previous option is no longer available. Since global knowledge of a network’s entanglement structure is often inaccessible, a successful protocol must operate with only a local knowledge of nodes and their entanglement. While entanglement status can be transmitted via classical communication, the process is slow and lends itself to system decoherence especially in a dynamic network. In this work, we introduce a multipartite entanglement routing protocol for dynamic networks, using DODAG trees and only a local knowledge of nodes. We detail the utility of DODAG trees in the following section.

2.5 DODAG Structure

Maintaining connectivity in a dynamic physical network is a non-trivial process in the NISQ (noisy intermediate-scale quantum) era. One proposal for combating information loss due to noise is the incorporation of a Destination Oriented Directed Acyclic Graph (DODAG) to preserve the virtual topology of the quantum network [17, 31]. The RPL protocol for classical networks, presented in [31], utilizes a DODAG for Low Power and Lossy Networks (LLNs) to facilitate efficient routing under a variety of classical network conditions. RPL optimizes energy consumption by dynamically adjusting the control message transmission rate, thus addressing topological inconsistencies during active data transmission phases. Nodes are organized in a hierarchy, with the root node serving as the central point for data aggregation and distribution.

For a quantum network, a DODAG dynamically maintains the virtual topology, allowing for real-time adaptation to changes in the physical and virtual network. Furthermore, preserving the virtual topology using a DODAG is a classical process and requires no additional quantum overhead [31]. We utilize power of a DODAG to preserve entanglement while performing measurements in our routing scheme. Figure 4 depicts a DODAG selected to maintain the entanglement structure in a 36-node quantum network.

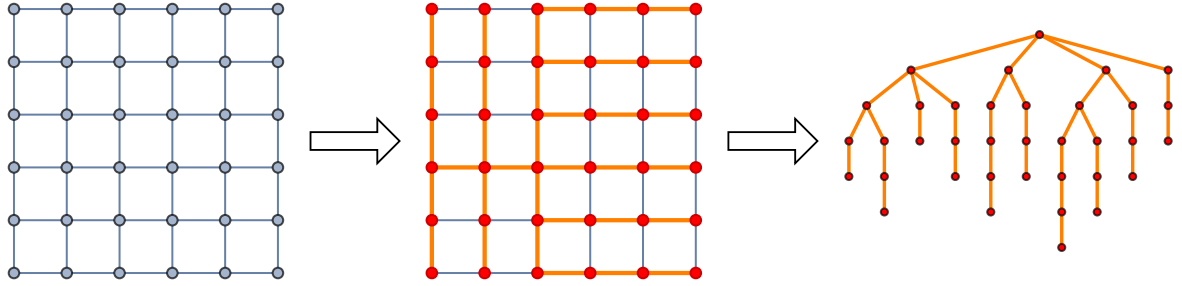


Figure 4: An initial physical network is shown to the left. We entangle parties with a DODAG tree, shown in red, which will preserve the virtual topology as we employ entanglement routing. The isolated DODAG is shown to the right.

Our protocol utilizes a non-greedy DODAG [23] to generate and maintain a virtual tree topology over different physical topologies. We assume a previous recurrent step where a DODAG protocol was introduced in the network, thereby forming an entangled tree structure among all nodes. Next, by associating a graph state to this resulting tree structure, we use a measurement based protocol to entangle any 3 specific parties within the virtual topology. We term this protocol DODAG-X, and discuss the details of the entanglement routing process in the next section.

3 DODAG-X Protocol

In this section we introduce the DODAG-X protocol for distributing multipartite entanglement across a quantum network. In our protocol, we incorporate a DODAG tree within the quantum network to maintain the virtual topology in time, allowing the physical topology to remain dynamic. We detail step-by-step instructions for performing the DODAG-X protocol, and provide computational packages to simulate entanglement routing with this scheme. Finally, we discuss the advantages of the DODAG-X protocol, and benchmark its performance against the well-known X-protocol, for various network topologies and party arrangements.

3.1 The Protocol

We now define the DODAG-X protocol for generating arbitrary entanglement among, up to, 3 parties in an n -party quantum network. We assume that a DODAG tree has been chosen for the network, with the root selected as a node of minimum eccentricity as described in Appendix A. The entire protocol is illustrated in Figure 5.

1. Given a DODAG on the physical network, determine $n \leq 3$ parties to entangle.
2. For each party $i \in \{n\}$ find the shortest path from that party's node to the root, denoted $P_{i,r} = \{v_1 = i, v_2, \dots, v_m = r\}$, where m is the length of the path. If a node v_j , with $v_j \neq r$, occurs in $P_{i,r}$ for all $i \in n$, set v_j as the new root.

3. For any pair of parties $\{i, j\}$, and associated paths $P_{i,r}$ and $P_{j,r}$, let $I_{i,j}$ denote the intersection of two path sequences

$$I_{i,j} \equiv P_{i,r} \cap P_{j,r}. \quad (9)$$

We define an *intersection node* to be the first element¹ $a_{i,j}(0)$ of the sequence $I_{i,j}$. We refer to $a_{i,j}(0)$ as $a_{i,j}$ going forward. We further note that $a_{i,j} = a_{j,i}$.

4. Entangle each party i with its nearest intersection node $a_{i,j}$. This is performed through the following steps:

- (a) For each party i , identify all² its intersection nodes $a_{i,j}$.
- (b) Identify the paths from i to each of its intersection nodes $a_{i,j}$, i.e. $P_{i,a_{i,j}}$ for all $j \neq i \in \{n\}$. The shortest such $P_{i,a_{i,j}}$, denoted $\bar{P}_{i,a_{i,j}}$, determines the nearest³ intersection node $a_{i,j}$ to i .
- (c) Perform sequential $X[v, w]$ measurements on each $v \in \bar{P}_{i,a_{i,j}}$, excluding $v = i$ and $v = a_{i,j}$, always using node $w = i$ (the party) for local complementation.

After Step 4, each party node will be connected to an intersection node, or is an intersection node itself. If a party node is also an intersection node, it will now be entangled with the root (see Theorem 1 in Appendix B).

5. Entangle all intersection nodes with the root. Here there are three possible cases:

- (a) There is 1 intersection node $a_{i,j}$ in the DODAG. Then $a_{i,j} = r$ and this step is complete.
- (b) There exists an intersection node $a_{i,j} \neq r$ in the DODAG, and $a_{i,j}$ is also party node. Then $a_{i,j}$ is connected to the root after Step 4, and this step is complete.
- (c) There exists an intersection node $a_{i,j}$ that is neither the root r , nor a party. We entangle $a_{i,j}$ with r using the following:

- i. Identify the path $P_{a_{i,j},r} = \{v_1 = a_{i,j}, v_2, \dots, v_m = r\}$, which we already know from $P_{i,r}$ in Step 2.
- ii. Perform $X[v_k, v_{k-1}]$ measurements on $v_k \in P_{a_{i,j},r}$, for all even k , excluding $v_k = a_{i,j}$ and $v_k = r$.
- iii. If $|P_{a_{i,j},r}|$ is even, perform a final $X[v_{m-1}, i]$ on the second-to-last vertex along $P_{a_{i,j},r}$, using the party i for local complementation.

6. If $r \in \{n\}$, i.e. the root is a party, the entangling protocol is complete. If $r \notin \{n\}$, we perform an $X[r, i]$ measurement where i is any party entangled⁴ with the root.

¹The root is a vertex shared by all $P_{i,j}$, and therefore is a minimum intersection for any two paths.

²For n parties there are, at most, $n - 1$ distinct intersection nodes for each party.

³The intersection node chosen is the first intersection encountered by a party on its path to the root.

⁴The situation where every party is not connected to the root after Step 5 can only occur if Step 5c was required. For this case the party i , the one entangled with $a_{i,j}$ in Step 5c, can always be used for local complementation in Step 6. Therefore, we emphasize that this protocol does not require an additional graph check during this step.

7. Perform a Z-Measurement on every node in the neighborhood of all parties, excluding the parties themselves. (see Appendix C)

After Steps 1–7 we are left with a maximally-entangled n -party state, for $n \leq 3$, that is not entangled with any other state in the network. The protocol requires a single graph check, and minimizes measurements needed for the entangling process. Steps 1–4, as written, apply generically for arbitrary party number. Steps 5–7 likewise generalize with an additional graph check. We provide an example of the DODAG-X protocol below.

Example: We now give an example of DODAG-X on a 6×6 grid, illustrated in Figure 5. Beginning with a DODAG tree, we select parties v_1 , v_2 , and v_3 to entangle. The path from each v_i to the root is computed, and intersection nodes, e.g. $a_{2,3}$, are identified (Figure 5a). We emphasize that this initial path-finding step is the only path-finding computation needed. Each v_i is entangled with its nearest intersection node using the X-protocol (Figure 5b). Intersection nodes are entangled with the root (Figure 5c) by X-measuring alternating nodes along each path as in Step 5. All nodes in the neighborhood of each party node, which are not party nodes themselves, are removed using Z-measurements (Figure 5d). This final step separates the entangled triplet from the rest of the graph.

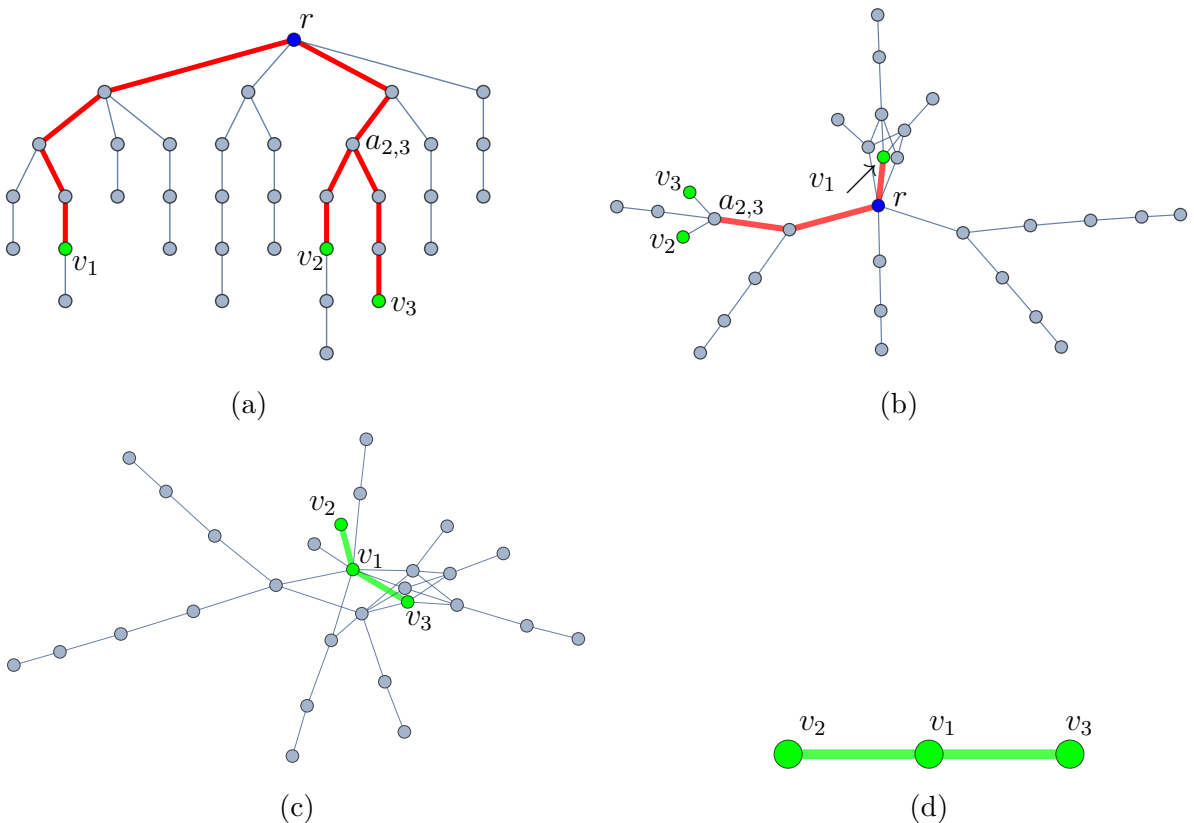


Figure 5: (a) Given a DODAG, parties to entangle are selected (in green) and the path from each party to the root is computed. (b) X measurements are performed on alternating nodes along each path, according to Step 4, entangling parties with their nearest intersection node. (c) Intersection nodes are then entangled with the root using Step 5. (d) Finally, all nodes non-party nodes are removed with Z measurements.

We demonstrated how the DODAG-X protocol generates entanglement between any 3 parties in an n -party network. Since the DODAG imposes a tree structure on the network a single path exists from each party to the root, thereby eliminating the need for multiple path-finding computations during the protocol. This reduction to the single path-finding calculation offers significant scaling advantages in classical complexity as the number of nodes grows large. Furthermore there are no additional graph checks required during the entangling protocol, minimizing interaction as the system evolves. In the next section we analyze deeper the complexity advantages of DODAG-X for different graph topologies.

3.2 Complexity in DODAG-X

Once a virtual topology has been formed by the DODAG, alternative approaches such as the X-protocol reviewed in Section 2.3 can be used to entangle parties in the network. However, these existing protocols require periodic verification of state of the physical network, and numerous path-finding steps using algorithms such as Dijkstra or Breadth-First-Scan (BFS) searches. Accordingly, these previous protocols are computationally inefficient since both Dijkstra and BFS have complexity $\mathcal{O}(n)$, for unweighted graphs of n vertices [32]. Instead it is computationally advantageous to using the DODAG hierarchy in place of path finding, thereby simplifying this first stage of the algorithm.

When entangling nodes in DODAG-X, we always measure along the unique path which connects each node to the root of the DODAG tree. Maximum path lengths are fixed by the depth of the tree which is set by the eccentricity of the root, a value minimized when initially determining the root node (see Appendix A). The initial path information is sufficient to complete the protocol, without auxiliary checks on the physical network. This approach consequently reduces maximal path lengths, and simultaneously eliminates the need for multiple path-finding searches. Once all parties of interest have been entangled with the root, a single X-measurement will entangle the parties with each other. We now analyze the performance of DODAG-X on two different topologies: grid lattice graphs and Small-World graphs, shown in Figure 6 below.

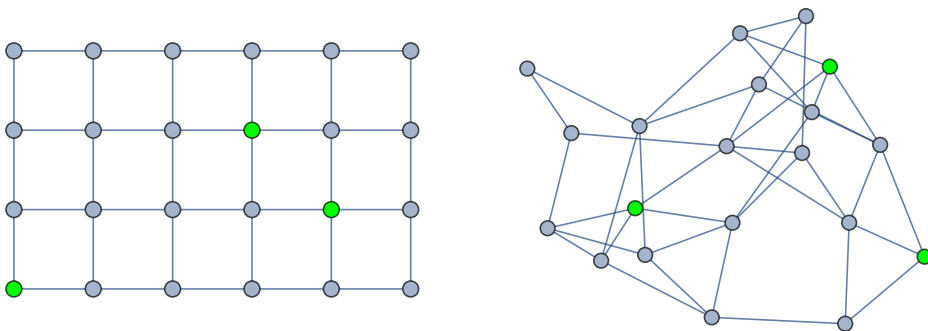


Figure 6: A grid of dimension 6×4 is shown to the left. For a grid of dimension $m \times \ell = n$, DODAG-X complexity scales between $\mathcal{O}(\sqrt{n})$ and $\mathcal{O}(n)$ depending on m/ℓ . For a Small-World graph, e.g. shown right, DODAG-X scales as $\mathcal{O}(\log n)$.

When performing the DODAG-X protocol on a grid of dimension $n = m \times \ell$, the ratio m/ℓ

affects the complexity scaling. When $m/\ell \approx 1$ the path-finding complexity of DODAG-X scales as $\mathcal{O}(\sqrt{n})$, as shown in Appendix A. Accordingly, for highly-symmetric quantum networks with grid topology, DODAG-X offers a factor of n improvement over existing protocols. For highly-asymmetric grid graphs, e.g. $m \gg \ell$, the performance of DODAG-X approaches the $\mathcal{O}(n)$ scaling of previous protocols such as the X-protocol.

The Small-World topology characterizes graphs of large clustering coefficient and low shortest-path distances. We construct Small-World graphs using the Watts-Strogatz model [33], beginning with a ring graph with parameter k denoting the mean vertex degree of all nodes. Edges are modified by attaching each node to a new node, chosen with probability p from a uniform distribution. The DODAG-X path-finding complexity scales as $\mathcal{O}(\log(n))$ in graphs with Small-World topology, again offering a strong improvement over previous protocols. Since many social networks, and even the network architecture of the internet itself, admit a Small-World structure, the DODAG-X protocol can significantly reduce overhead in a realistic quantum network.

In this section we described the computational complexity of DODAG-X when compared to existing entanglement routing schemes. We specifically focus on two candidate topologies for a real quantum network, namely the grid and Small-World topologies, and demonstrate the improved scaling of DODAG-X in both cases. These improvements rely on the initial tree structure imposed by the DODAG, which pre-selects the shortest path from each node to the root, thereby eliminating the need for numerous graph checks and path-finding calculations. Further details for each claim can be found in Appendix A, and performance benchmarks are given throughout Section 4. In the next section we discuss generalizations of DODAG-X to arbitrary party number.

3.3 Generalizations to Higher Party Number

As discussed in Section 3.1, Steps 1–4 of the DODAG-X protocol generalize to arbitrary parties in an n -party network. Stated explicitly, given a DODAG tree on some n -party quantum network we can successfully entangle m parties with each of their nearest intersection nodes by applying Step 4 of the DODAG-X protocol. Accordingly, we can entangle any m parties using DODAG-X if their only shared intersection node is the root. Figure 7 below depicts an example for entangling 4 parties.

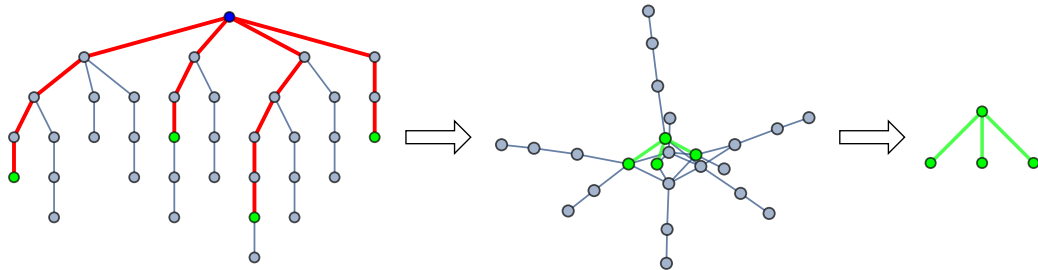


Figure 7: The DODAG-X protocol can entangle an arbitrary number of parties when the parties lie along distinct branches of the DODAG tree, as in the 4-party example above.

Step 5 of the DODAG-X protocol does not completely generalize to m -party entangle-

ment. However, for many non-trivial cases the protocol succeeds in generating the desired m -party state. Figure 8 displays a few examples where the DODAG-X protocol can generate higher-party entangled states, even when the parties do not lie in separate branches of the DODAG tree. We believe the DODAG-X protocol to generalize when , but leave further analysis for future work.

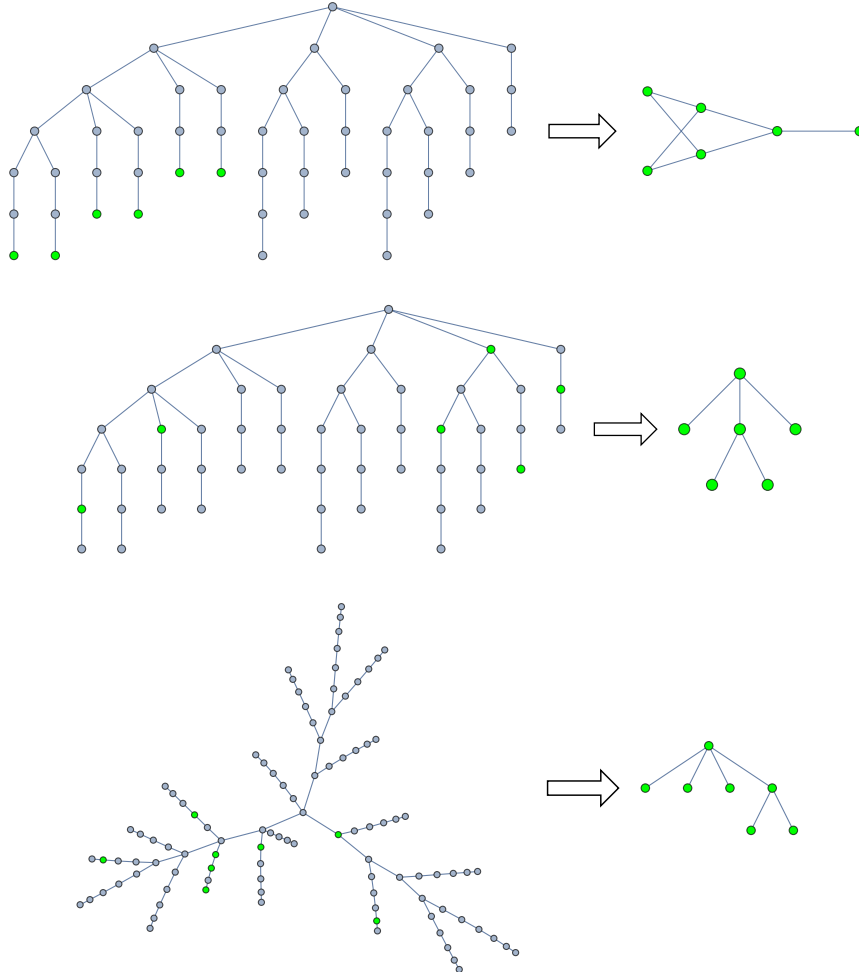


Figure 8: Even when parties do not lie in separate branches of the DODAG, the DODAG-X protocol can successfully produce entanglement among arbitrary parties in many cases.

In this section we introduced the DODAG-X protocol for entanglement routing in a quantum network. We demonstrated the utility of establishing an initial DODAG tree, which maintains the virtual topology in time and reduces path-finding complexity. We analyzed the scaling of DODAG-X as the quantum network grows large, specifically for graphs with a grid and Small-World topology. We compared the scaling complexity of DODAG-X to previous entanglement routing schemes, and showed improved scaling for both topologies. Furthermore, we discussed the cases when DODAG-X can generate arbitrary party entanglement. In the next section we benchmark DODAG-X against the X-protocol, comparing the number of measurements needed to complete each protocol.

4 Performance Benchmarks

In the previous section we demonstrated that DODAG-X significantly reduces the number of path-finding computations, offering a scaling advantage over preexisting protocols. Integral to the success of DODAG-X is the establishment of a DODAG tree, which maintains the virtual topology in time despite changes to the physical network. We now illustrate how implementing this DODAG tree minimizes the number of measurements needed to entangle chosen parties in the network. We explicitly benchmark the performance of DODAG-X when compared to the X-protocol, emphasizing the utility of a tree in the virtual topology, for physical networks with grid and Small-World topologies.

We consider a physical network with nodes we wish to entangle. We generate a DODAG on which the DODAG-X protocol will be performed, and apply the X-protocol directly⁵ on the physical network. The number of measurements needed to entangle all combinations of three parties is computed, and the average number of measurements is subsequently extracted. We perform this calculation for physical networks of varying size and symmetry. The percentage differences in performance are computed according to

$$\frac{\overline{M}_p - \overline{M}_v}{\overline{M}_p} \times 100, \quad (10)$$

where \overline{M}_p denotes the average measurements needed for the X-protocol on the physical network, and \overline{M}_v the measurements needed for DODAG-X in the virtual topology.

4.1 Grid Lattice Networks

We begin with grid lattice network, which can be completely characterized by its number of rows m and columns ℓ . We analyze networks with $n = m \times \ell$ nodes, for $4 \leq n \leq 81$. The relative size of m and ℓ determines the asymmetry of the lattice, and we explore all cases where $2 \leq m \leq 9$ and $2 \leq \ell \leq 9$. Figure 9 presents heat maps for the average number of measurements required to conduct the X-protocol on the physical network, compared to DODAG-X on the virtual topology.

For all grid networks in Figure 9, with the sole exception of 3×3 grids, DODAG-X requires fewer measurements on average to entangle any three parties than the X-protocol. As the number of nodes increases, the improved performance of DODAG-X becomes more and more significant. This improvement is largely due to the fact that the DODAG reduces neighborhood size by facilitating node isolation, reducing the number of final Z-measurements needed to disconnect the final entangled state from the rest of the network. Furthermore, the embedded DODAG tree retains internode path lengths comparable to those of the initial grid. Figure 9 illustrates a direct comparison between the two protocols, plotting the percent difference of average measurements as defined in Eq. (10).

⁵If the physical network is a tree, the number of measurements to complete DODAG-X and the X-protocol are equal (Appendix C).

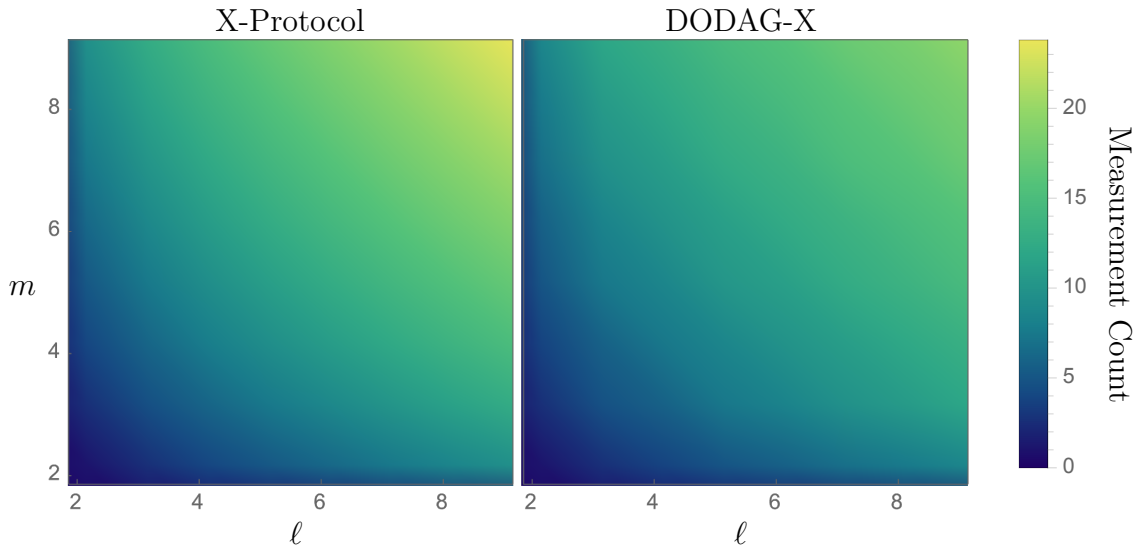


Figure 9: Left shows the average measurements needed to complete the X-protocol directly on the physical network. Right gives the average measurements to complete the DODAG-X protocol on a virtual DODAG embedded in the same physical network.

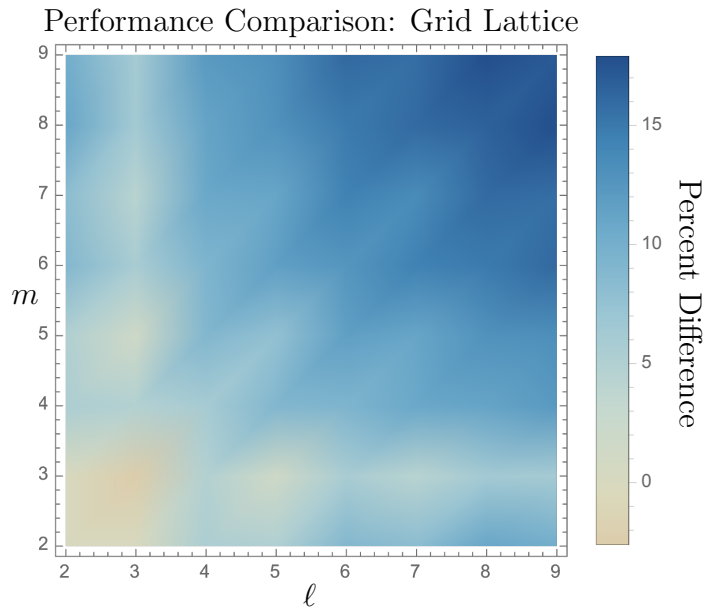


Figure 10: Percent difference of measurements between DODAG-X and X-protocol for grid networks. Blue shows improved performance of DODAG-X compared to X-protocol. Red indicates worse performance by DODAG-X, and white shows identical performance.

As shown in Figure 10, incorporating a DODAG structure on the physical network offers significant reduction in overall measurements when entangling three parties. In particular, for larger networks and networks with high levels of symmetry, we find that DODAG-X enables up to 17.87% fewer measurements on average. For the single case of a 3×3 grid, we find that the DODAG may result in up to 2.62% more measurements on average.

We emphasize that the selection of the initial DODAG is important for the resource impact of the protocol. While we utilize a breadth-first-scan technique, from an initial node of minimum eccentricity, this construction may not be optimal for all physical

networks. Furthermore, the process of optimizing over all DODAG trees given a physical network is a complex question which warrants consideration, and which we leave for future work. We now analyze performance on physical networks with Small-World topology.

4.2 Small-World Networks

We now conduct a performance analysis on networks with Small-World topology. Recall from Section 3.2 that Small-World graphs, in the Watts-Strogatz construction, are parameterized by the mean vertex degree k of the initial ring, and the probability of node rewiring p . We consider networks with $n = 30$ nodes, and evaluate both protocols for pairs $\{k, p\}$ with $2 \leq k \leq 24$ and $0 \leq p \leq 1$. Figure 11 gives a heat map for the average number of measurements needed to entangle all possible node triplets using the DODAG-X protocol on the virtual topology, and the X-protocol on the physical network.

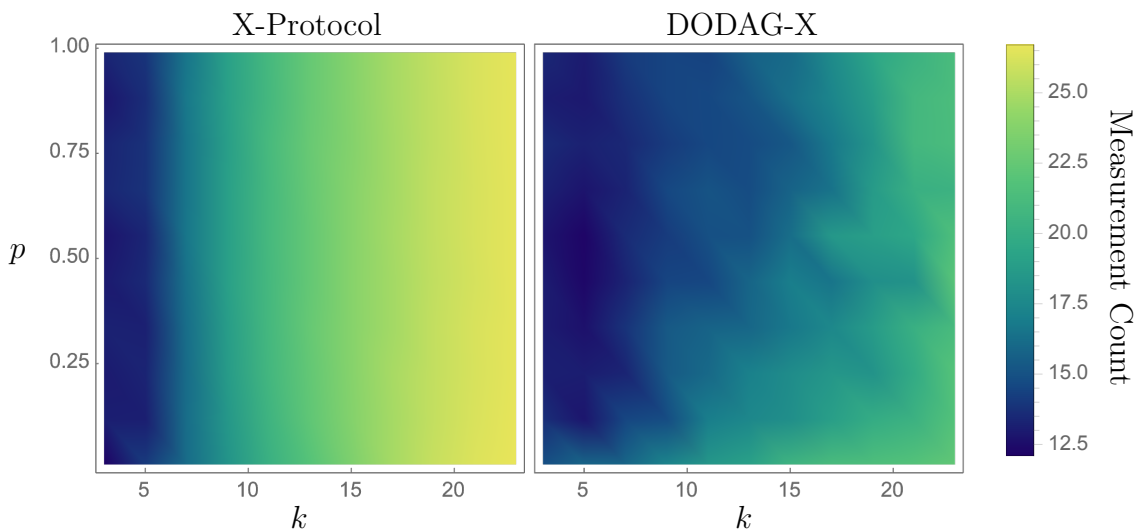


Figure 11: Average measurements to entangle all triplets in Small-World networks of $n = 30$ nodes with mean degree k and rewire probability p . Left shows DODAG-X performance on virtual topology, while right shows X-protocol on the physical network.

For Small-World graphs with high clustering coefficient, set by k , the DODAG-X protocol significantly out-performs the X-protocol. The improvement becomes more noticeable as k grows large, where vertex neighborhoods experience greater edge modification upon local complementation. The X-protocol is consistent up to change in rewiring probability p , while DODAG-X experiences a slight decrease in performance for small p values. Figure 12 illustrates the percent difference in performance when implementing DODAG-X over the X-protocol on networks with Small-World topology.

Over all Small-World networks considered, the DODAG-X protocol requires an average of 20%–25% less measurements when compared to the X-protocol operating on the physical topology. In certain cases with high clustering coefficient and high rewiring probability, this improvement reaches up to 35%. For stable weakly-clustered networks, very low k and p , implementing the virtual DODAG can be unfavorable compared to acting directly

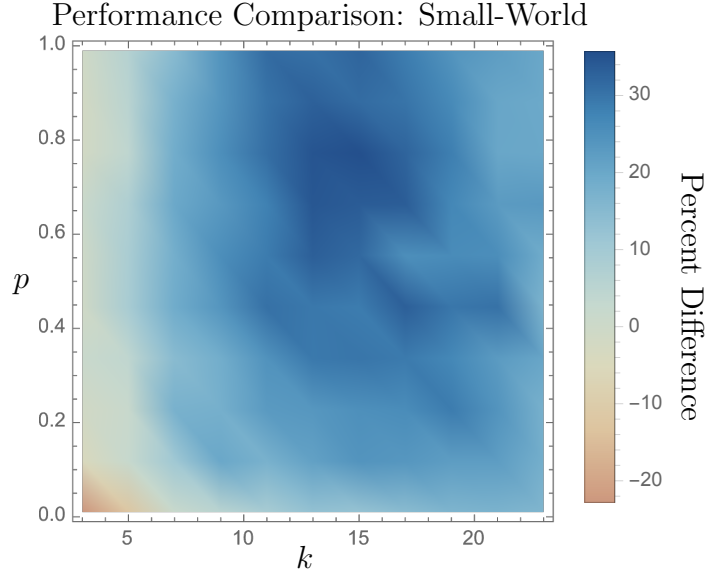


Figure 12: Percent difference of average measurements to entangle three parties with DODAG-X compared to X-protocol. Small-World graphs with $n = 30$ nodes are considered, with initial mean vertex degree k and rewiring probability p .

on the physical network, requiring 10% more measurements on average. Around $k = 8$ we observe that DODAG-X performs significantly better, on average, for all p .

We seek to better understand the impact of parameter p on the required measurements for each protocol. Accordingly, we benchmark the performances of DODAG-X and the X-protocol on Small-World graphs of fixed clustering k . Figure 13 shows the average measurements needed to entangle three parties when $k = 9$, where rewiring probability p and node count N are varied. Additional fixed k plots are given in Appendix D.

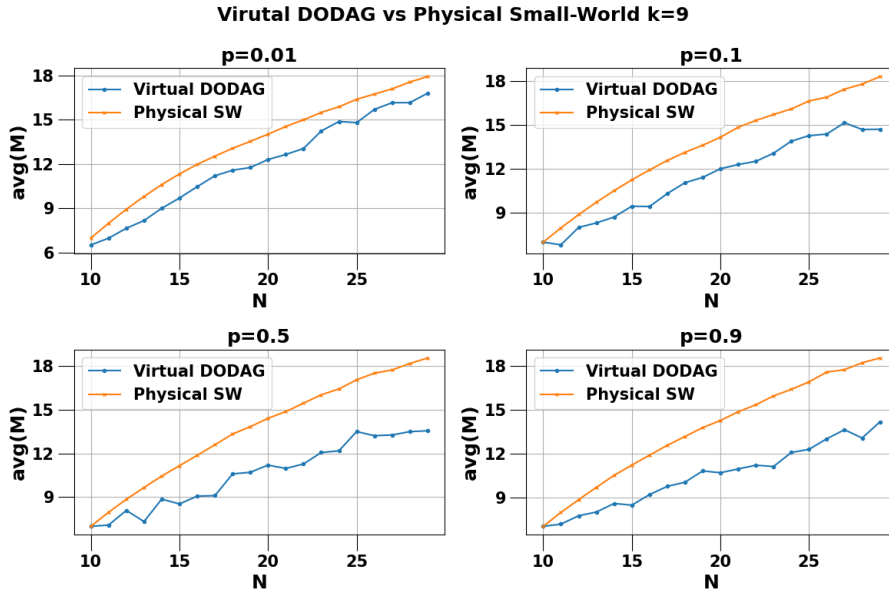


Figure 13: DODAG-X and X-protocol on Small-World graphs of fixed clustering k . DODAG-X requires less average measurements as rewiring probability p is increased.

In Figure 13 we observe that for low values of p , corresponding to low connectivity between distant nodes, implementing the virtual DODAG yields similar performance to the X-protocol on the physical network for all N . However as the value of p increases, the improved efficiency of DODAG-X can be observed as N grows larger. This improvement owes itself to the DODAG construction, which minimizes path distance from any node to the root by maximizing the number of branches in the tree. Consequently, the number of required measurements along each path is likewise minimized, as is the number of isolation measurements needed at the end of the protocol.

In this section we analyzed how implementing a DODAG tree in the physical quantum network affects entanglement routing performance. We directly compared the average number of measurements required to entangle parties using the DODAG-X protocol on the virtual DODAG tree, compared to the X-protocol applied directly on the physical network. Specifically, we focused on physical networks with grid lattice and Small-World topologies. For grid graphs we demonstrated that DODAG-X offers significant measurement reduction for large networks, as well as networks with a high level of lattice symmetry. Similarly for the case of Small-World networks, the DODAG-X protocol outperformed the X-protocol in almost all cases, with largest improvements coming from networks with high clustering and high rewiring probability. Finally, we analyzed the effect of rewiring probability in Small-World networks on the DODAG tree construction. We will now conclude with a discussion of results and future research directions.

5 Discussion and Future Work

In this work we presented the DODAG-X protocol for entanglement routing in quantum networks. The protocol began by constructing a DODAG, a topology-preserving spanning tree on the physical network, and selecting parties to entangle. Next, the path from each party node to the graph root is identified, along with intersection nodes encountered along the way. Employing a variation of the standard X-protocol, we entangle each party node with its respective nearest intersection node, and then entangle all intersection nodes with the singular root. A final X-measurement is performed at the root node to entangle all parties, and remaining non-party nodes are measured away. The resultant system is a multipartite entangled state, consisting of only the selected parties of interest.

There are several notable advantages gained from incorporating a DODAG protocol into an entanglement routing scheme. First, since the DODAG is a spanning tree by construction, all graph paths from the party nodes to the root are calculated using an initial classical computation. This prominent feature eliminates the need for successive graph checks while performing the entangling protocol, reducing potential interference with the sensitive quantum system. Additionally, the DODAG preserves connections in the physical network using only classical processes [17], thereby mitigating information loss due to noisy hardware. As a result, entanglement can be distributed throughout the network much faster than the decoherence time of the constituent qubits. This semi-classical approach enables non-trivial quantum processes to be performed on contemporary NISQ (noisy intermediate scale quantum) hardware.

While the DODAG-X protocol was designed to establish three-party entanglement in an

n -party network, the procedure generalizes for many useful cases at higher party number (see Figure 8). For example, if m parties exist as the leaves of m distinct branches in the DODAG tree, all m parties can be brought into a single entangled state with a single application of the DODAG-X protocol. Furthermore, so long as intersection nodes do not share significant⁶ path intersection to the root, the DODAG-X protocol likewise generalizes to m parties.

When a single application of DODAG-X is not sufficient to generate arbitrary m -party entanglement, a concatenated protocol can be applied to yield the desired state. For example, if we extend the DODAG to support multiple qubits per node we generate a multi-layer tree structure. Each layer may then be treated as a separate instance of the network, allowing the DODAG-X protocol to be applied independently layer-by-layer. We select m parties to entangle, and build $\lceil m/3 \rceil$ layers with corresponding roots. We perform DODAG-X on each layer to bring all parties into an entangled state with their respective roots, and entangle all roots using fusion methods like those presented in [34]. This concatenated approach, while potentially less efficient at very large scales, offers one solution for generating arbitrary multipartite entanglement in generic network topologies.

In this work we focus on entanglement routing in a quantum network, however, there exist numerous quantum properties whose distribution may be explored through a similar lens. One such property of immediate interest is quantum magic [35, 36, 37], a measure of non-stabilizerness in a quantum system. The amount of magic directly impacts the difficulty of classically simulating that system. It has been demonstrated that non-local magic, the magic supported in quantum correlations, is intimately tied to the entanglement structure of a many-body system [38, 39]. Following this, the notion of *magic routing* in a quantum network could likewise be explored using the DODAG-X protocol.

Graph states, mathematically equivalent to the quantum networks studied in this paper, admit a dual description in a group-theoretic formalism [40, 41, 42, 43]. As a result, we can utilize group-theoretic techniques and proofs to analyze global properties and capabilities of quantum networks. In [44] it was shown how certain groups of entangling operations exactly constrain the possible entanglement structures in a multipartite quantum system. A similar analysis can be performed for quantum networks, and analogous constraints derived, by analyzing the composition of the constituent channels. Furthermore, entanglement rates in arbitrary network channels can likewise be explored following the work of [45].

6 Acknowledgements

The authors thank Dr. Ze-Xun Lin for his support and advice. We gratefully acknowledge funding from the National Science Foundation (NSF) under NSF Award 2137828 “QuIC-TAQS: Deterministically Placed Nuclear Spin Quantum Memories for Entanglement Distribution”, NSF Award 2246394 “CAREER: First Principles Design of Error-Corrected Solid-State Quantum Repeaters”, and NSF Award 2107265 “U.S.-Ireland R&D

⁶When the path from an intersection node to the root contains multiple other intersection nodes in the network, a single application of DODAG-X does not guarantee a final m -party entangled state. For all other cases, we expect the DODAG-X protocol to generalize.

Partnership: Collaborative Research: CNS Core: Medium: A unified framework for the emulation of classical and quantum physical layer networks”. P.N. acknowledges Grant No. GBMF8048 from the Gordon and Betty Moore Foundation.

Code and Data Availability

Relevant code and data from this study are available upon request.

References

- [1] C. Thalacker, F. Hahn, J. de Jong, A. Pappa and S. Barz, *Anonymous and secret communication in quantum networks*, *New Journal of Physics* **23** (2021) 083026.
- [2] M. Belghachi, *Quantum networks: Emerging research areas, challenges, and opportunities*, .
- [3] S. Wengerowsky, S. K. Joshi, F. Steinlechner, J. R. Zichi, S. M. Dobrovolskiy, R. Van der Molen et al., *Entanglement distribution over a 96-km-long submarine optical fiber*, *Proceedings of the National Academy of Sciences* **116** (2019) 6684.
- [4] H. Kaushal, V. Jain and S. Kar, *Free space optical communication*, vol. 60. Springer, 2017.
- [5] A. Kolar, A. Zang, J. Chung, M. Suchara and R. Kettimuthu, *Adaptive, continuous entanglement generation for quantum networks*, in *IEEE INFOCOM 2022-IEEE Conference on Computer Communications Workshops (INFOCOM WKSHPS)*, pp. 1–6, IEEE, 2022.
- [6] C. Macchiavello and G. M. Palma, *Entanglement-enhanced information transmission over a quantum channel with correlated noise*, *Physical Review A* **65** (2002) 050301.
- [7] N. Skjellum, M. Shaban and M. Ismail, *Secure and efficient entanglement distribution protocol for near-term quantum internet*, *arXiv preprint arXiv:2312.05775* (2023) .
- [8] S. Pouryousef, N. K. Panigrahy and D. Towsley, *A quantum overlay network for efficient entanglement distribution*, in *IEEE INFOCOM 2023-IEEE Conference on Computer Communications*, pp. 1–10, IEEE, 2023.
- [9] Y. Zhang, Z. Li, C. Weedbrook, K. Marshall, S. Pirandola, S. Yu et al., *Noiseless linear amplifiers in entanglement-based continuous-variable quantum key distribution*, *Entropy* **17** (2015) 4547.
- [10] S. Pirandola, *End-to-end capacities of a quantum communication network*, *Communications Physics* **2** (2019) 51.
- [11] M. Hein, W. Dür, J. Eisert, R. Raussendorf, M. Nest and H.-J. Briegel, *Entanglement in graph states and its applications*, *arXiv preprint quant-ph/0602096* (2006) .
- [12] E. S. Cooper, P. Kunkel, A. Periwal and M. Schleier-Smith, *Graph states of atomic ensembles engineered by photon-mediated entanglement*, *Nature Physics* (2024) 1.
- [13] Z. Li, H. Zhu and M. Hayashi, *Robust and efficient verification of graph states in blind measurement-based quantum computation*, *npj Quantum Information* **9** (2023) 115.
- [14] P. Hilaire, E. Barnes, S. E. Economou and F. Grosshans, *Error-correcting entanglement swapping using a practical logical photon encoding*, *Physical Review A* **104** (2021) 052623.

- [15] J. I. Cirac, A. Ekert, S. F. Huelga and C. Macchiavello, *Distributed quantum computation over noisy channels*, *Physical Review A* **59** (1999) 4249.
- [16] N. Shettell and D. Markham, *Graph states as a resource for quantum metrology*, *Physical review letters* **124** (2020) 110502.
- [17] Z. Yang, A. Ghubaish, R. Jain, H. Shapourian and A. Shabani, *Asynchronous entanglement routing for the quantum internet*, *AVS Quantum Science* **6** (2023) .
- [18] F. Hahn, A. Pappa and J. Eisert, *Quantum network routing and local complementation*, *npj Quantum Information* **5** (2019) 76.
- [19] V. Mannalath and A. Pathak, *Multiparty entanglement routing in quantum networks*, *Physical Review A* **108** (2023) 062614.
- [20] A. Sen, K. Goodenough and D. Towsley, *Multipartite entanglement distribution in quantum networks using subgraphs complementations*, *arxiv preprint quant-ph:2308.13700* (2024) .
- [21] X. Fan, C. Fan, H. Gupta and C. Ramakrishnan, *Optimized distribution of entanglement graph states in quantum networks*, *arxiv preprint quant-ph:2405.00222* (2024) .
- [22] C. Meignant, D. Markham and F. Grosshans, *Distributing graph states over arbitrary quantum networks*, *Phys. Rev A* **100** (2019) .
- [23] R. Alexander, A. Brandt, J. Vasseur, J. Hui, K. Pister, P. Thubert et al., “RPL: IPv6 Routing Protocol for Low-Power and Lossy Networks.” RFC 6550, Mar., 2012. 10.17487/RFC6550.
- [24] A. Ehrenfeucht, T. Harju and G. Rozenberg, *Transitivity of local complementation and switching on graphs*, *Discrete mathematics* **278** (2004) 45.
- [25] E. Kaur, A. Patil and S. Guha, *Resource-efficient and loss-aware photonic graph state preparation using an array of quantum emitters, and application to all-photonic quantum repeaters*, *arXiv preprint arXiv:2402.00731* (2024) .
- [26] A. Kay, J. K. Pachos and C. S. Adams, *Graph-state preparation and quantum computation with global addressing of optical lattices*, *Physical Review A* **73** (2006) 022310.
- [27] M. Van den Nest, J. Dehaene and B. De Moor, *Graphical description of the action of local clifford transformations on graph states*, *Physical Review A* **69** (2004) 022316.
- [28] M. Hein, J. Eisert and H. J. Briegel, *Multiparty entanglement in graph states*, *Physical Review A* **69** (2004) 062311.
- [29] A. Dahlberg and S. Wehner, *Transforming graph states using single-qubit operations*, *Philosophical Transactions of the Royal Society A: Mathematical, Physical and Engineering Sciences* **376** (2018) 20170325.

- [30] W. Kozłowski, A. Dahlberg and S. Wehner, *Designing a quantum network protocol*, in *Proceedings of the 16th international conference on emerging networking experiments and technologies*, pp. 1–16, 2020.
- [31] J. Vasseur, N. Agarwal, J. Hui, Z. Shelby, P. Bertrand and C. Chauvenet, *Rpl: The ip routing protocol designed for low power and lossy networks*, *Internet Protocol for Smart Objects (IPSO) Alliance* **36** (2011) 1.
- [32] D. S. Ashish, S. Munjal, M. Mani and S. Srivastava, *Path finding algorithms*, in *Emerging Technologies in Data Mining and Information Security: Proceedings of IEMIS 2020, Volume 1*, pp. 331–338, Springer, 2021.
- [33] D. J. Watts and S. H. Strogatz, *Collective dynamics of ‘small-world’ networks*, *nature* **393** (1998) 440.
- [34] X. Fan, C. Zhan, H. Gupta and C. Ramakrishnan, *Optimized distribution of entanglement graph states in quantum networks*, *arXiv preprint arXiv:2405.00222* (2024) .
- [35] S. Bravyi and A. Kitaev, *Universal quantum computation with ideal Clifford gates and noisy ancillas*, *Phys. Rev. A* **71** (2005) 022316 [quant-ph/0403025].
- [36] S. F. E. Oliviero, L. Leone and A. Hamma, *Magic-state resource theory for the ground state of the transverse-field Ising model*, *Phys. Rev. A* **106** (2022) 042426 [2205.02247].
- [37] S. F. E. Oliviero, L. Leone, A. Hamma and S. Lloyd, *Measuring magic on a quantum processor*, *npj Quantum Inf.* **8** (2022) 148 [2204.00015].
- [38] N. Bao, C. Cao and V. P. Su, *Magic state distillation from entangled states*, *Physical Review A* **105** (2022) .
- [39] C. Cao, G. Cheng, A. Hamma, L. Leone, W. Munizzi and S. F. E. Oliviero, *Gravitational back-reaction is magical*, 2403.07056.
- [40] M. Hein, W. Dür, J. Eisert, R. Raussendorf, M. Van den Nest and H. J. Briegel, *Entanglement in Graph States and its Applications*, 2, 2006, quant-ph/0602096.
- [41] C. Keeler, W. Munizzi and J. Pollack, *Entropic lens on stabilizer states*, *Phys. Rev. A* **106** (2022) 062418 [2204.07593].
- [42] C. Keeler, W. Munizzi and J. Pollack, *Clifford orbits from cayley graph quotients*, *Quant. Inf. Comput.* **24** (2024) 0001 [2306.01043].
- [43] F. Latour and O. Perdomo, *Five-qubit states generated by Clifford gates*, 2210.17034.
- [44] C. Keeler, W. Munizzi and J. Pollack, *Bounding Entanglement Entropy with Contracted Graphs*, 2310.19874.
- [45] J. Couch, S. Eccles, P. Nguyen, B. Swingle and S. Xu, *Speed of quantum information spreading in chaotic systems*, *Phys. Rev. B* **102** (2020) 045114 [1908.06993].

A Path-Finding Complexity

An optimal root for the DODAG-X protocol can be determined using only information about the initial physical network, thereby eliminating the need for any dynamic path-finding computations during the protocol. One viable method for selecting a suitable root is to minimize over the eccentricity of all vertices in the physical network. For a graph G and vertex $v \in G$, the eccentricity of v is calculated using

$$\text{Ecc}(G, v) = \max_{u \in G} \{d(v, u)\}, \quad (11)$$

where $d(v, u)$ indicates the distance of the shortest path connecting v and u in G . To select a root, we evaluate $\text{Ecc}(G, v)$ for all $v \in G$ and choose the vertex of lowest eccentricity to serve as the root. The complexity of finding paths from any party to the root then depends only on the depth of the DODAG tree.

When performing the DODAG-X protocol on a grid graph, the complexity of path-finding is determined by the asymmetry of the grid. For a graph of n vertices arranged in an $m \times \ell$ grid, the largest asymmetry occurs when either m or ℓ , but not both, is equal to 1. In this case, the depth of a spanning tree is given by $\frac{n}{2}$, and finding a path to the root occurs with $\mathcal{O}(n)$. Alternatively, when $m = \ell$ a spanning tree can have maximal depth $\frac{m}{2}$. Finding a path in this case requires only $\mathcal{O}(\sqrt{n})$. All other combinations of m and ℓ yield path-finding complexities between $\mathcal{O}(\sqrt{n})$ and $\mathcal{O}(n)$.

For a graph G with n vertices, a small-world topology can be defined using the Watts-Strogatz model [33]. In this small-world description, depth complexity is determined by two parameters, k and p . Parameter k denotes the mean vertex degree in a regular ring lattice of size n , and $0 \leq p \leq 1$ defines a rewiring probability on the ring lattice. It was also shown in [33], however, that the average distance $d(v, u)$ between randomly chosen nodes is proportional to $\log(n)$. Accordingly, the average depth complexity after employing a small-world topology goes as $\mathcal{O}(\log n)$.

B Proofs of Connectivity

In this section, we provide several important proofs that underlie the effectiveness of the DODAG-X protocol. Notation used below is first presented in Section 2.1.

One useful feature of tree graphs is the fact that, given a path $P \equiv \{v_1, v_2, \dots, v_m\}$, the neighborhoods of any v_n and v_{n+2} share a single vertex v_{n+1} . Otherwise stated, for any tree graph

$$N_{v_n} \cap N_{v_{n+2}} = \{v_{n+1}\}, \quad \forall n \in [1, m - 2]. \quad (12)$$

We utilize this feature below.

B.1 Proofs of Entangled Intersections

Theorem 1 *After entangling all party nodes $i \in \{n\}$ with their nearest intersection nodes $a_{i,j}$, each party node will either be connected to an intersection node, or be an intersection node itself.*

The first statement in Theorem 1, ensuring that all party nodes are connected to an intersection node, follows directly from the proof of connectivity given in [18]. The DODAG-X protocol begins with sequential X-measurements along the paths $P_{i,a_{i,j}} = \{v_1 = i, v_2, \dots, v_m = a_{i,j}\}$, without measuring i or $a_{i,j}$. This step is equivalent to the X-protocol presented in [18], where it was shown that any node, e.g. i , can be connected to any other node, e.g. $a_{i,j}$, by performing sequential X-measurements on all nodes comprising the shortest path between the two end nodes.

A more nuanced case occurs when a party node is also an intersection node, i.e. $i = a_{j,k}$ for some⁷ $i, j, k \in \{n\}$. We must keep track of the neighborhood N_i while performing measurements along the path $P_{i,a_{i,m}}$, from i to its nearest intersection node⁸ $P_{i,a_{i,m}}$, since this neighborhood will contain another party. We will therefore demonstrate that N_i is connected to an intersection node after all measurements have been performed.

For this we extend on the analysis of [18] and [19], describing the effects of subsequent X-measurements on a vertex neighborhood N_v . We begin with Appendix Eqs. 8–12 of [18], from which we can derive a simplified expression for $N_{v_1}^{(m-2)}$ as

$$N_{v_1}^{(m-2)} = \begin{cases} N_{m-1}^{(0)} \Delta \left(N_{m-3}^{(0)} \Delta \left(\dots \Delta \left(N_3^{(0)} \Delta N_1^{(0)} \right) \right) \right), & \text{for } m \text{ even} \\ N_{m-1}^{(0)} \Delta \left(N_{m-3}^{(0)} \Delta \left(\dots \Delta \left(N_4^{(0)} \Delta N_2^{(0)} \setminus \{v_1\} \right) \right) \right), & \text{for } m \text{ odd} \end{cases}, \quad (13)$$

where Δ above represents the symmetric difference operation, defined

$$A \Delta B \equiv (A \cup B) \setminus (A \cap B). \quad (14)$$

Likewise for $N_{v_m}^{(m-2)}$, we derive the form

$$N_{v_m}^{(m-2)} = \begin{cases} N_m^{(0)} \Delta \left(N_{m-2}^{(0)} \Delta \left(\dots \Delta \left(N_4^{(0)} \Delta N_2^{(0)} \right) \right) \right), & \text{for } m \text{ even} \\ \{v_1\} \cup \left(N_m^{(0)} \Delta \left(N_{m-2}^{(0)} \Delta \left(\dots \Delta \left(N_3^{(0)} \Delta N_1^{(0)} \right) \right) \right) \right), & \text{for } m \text{ odd} \end{cases}. \quad (15)$$

After $m - 2$ measurements, and utilizing Eq. (12), the set $N_{v_1=i}^{(0)} \setminus \{v_2\}$ will always be contained in either $N_{v_m=a_{i,j}}^{(m-2)}$ or $N_{v_1=i}^{(m-2)}$, depending on whether m is odd or even, respectively. As a result, the party node k , which initially had i as its intersection, will now be connected either party node i or intersection node $a_{i,j}$, but since both are intersections themselves, k will always be connected to an intersection. □

Corollary 1.1 *When entangling three parties with DODAG-X, if an intersection node is also a party node then it will be entangled with the root after Step 1.*

For n vertices in a tree graph, there can be at most $n - 1$ intersection nodes. When entangling 3 parties, we can therefore have at most 2 distinct intersection nodes in the network. Furthermore, since we have a tree structure, the root of the tree must be one of the 2 possible intersection nodes. Therefore if an intersection node is also a party node,

⁷We emphasize that i, j , and k need not all be distinct. This case applies equally when $i = j$ or $i = k$.

⁸For the three-party case, intersection node $a_{i,m}$ will always be the root of the DODAG tree.

its nearest intersection node will be the root, and it will be entangled with the root after performing the entangling procedure described in Theorem 1. □

B.2 Proof of Entangled Pairs

We can likewise use Eqs. (13)–(15) to prove that DODAG-X successively entangles any chosen pair v_i and v_j using at most $m - 2$ measurements, where m is the shortest path length $|P_{i,j}|$. In order to prove entanglement of the pair, we need to show $v_i \in N_{v_j}^{(m-2)}$ after the protocol has been applied.

If m is odd it is trivial to see $v_i \in N_{v_j}^{(m-2)}$, since Eq. (15), after identifying $v_i \rightarrow v_1$ and $v_m \rightarrow v_j$, gives $N_{v_j}^{(m-2)}$ as a union of sets with $\{v_i\}$. If m is even, we know $v_i \in N_2^{(0)}$ by construction of the path $P_{i,j}$. Additionally, $v_i \notin N_j^{(0)} \quad \forall k \neq 2$ by Eq. (12). Therefore v_i exists in the union of $N_2^{(0)}$ with any other set, but never exists in the intersection of any two sets $N_k^{(0)} \cap N_l^{(0)}$. Consequently v_i is always included, and never removed, under the symmetric difference operation, and thus we always have $v_i \in N_{v_j}^{(m-2)}$. □

B.3 Proof of Isolated Entangled Triplets

Theorem 2 *The DODAG-X protocol always results in three parties entangled with each other, and not entangled with any other node in the network.*

After applying Step 1 of the DODAG-X protocol, we are left with three possibilities discussed in Steps 5a, 5b, and 5c. The cases described in Steps 5a and 5b do not require additional measurement. In Step 5a, all parties are entangled with the root after Step 1, but not necessarily entangled with each other. For Step 5b, when intersection node $a_{i,j}$ is also a party, the node $a_{i,j}$ will already be entangled with the root following Step 1. Both cases above are proved using Theorem 1.

For Step 5c, we consider an intersection node $a_{i,j}$ that is neither the root nor a party node. By examining the neighborhoods $N_{a_{i,j}}^{(0)}$ and $N_r^{(0)}$, and dividing the path $P_{a_{i,j},r}$ into smaller pieces, we can track the effects of sequential measurements on alternating nodes. Given $P_{a_{i,j},r} = \{v_1, \dots, v_m\}$, after an X-measurement on v_2 we have

$$\begin{aligned} N_{v_1}^{(v_2)} &= N_{v_2}^{(0)} \setminus \{v_1\}, \\ N_{v_3}^{(v_2)} &= \{v_1\} \cup (N_{v_3}^{(0)} \Delta N_{v_1}^{(0)}). \end{aligned} \tag{16}$$

Similarly, after performing an X-measurement on v_4 we have

$$\begin{aligned} N_{v_3}^{(v_4)} &= N_{v_4}^{(0)} \setminus \{v_3\}, \\ N_{v_5}^{(v_4)} &= \{v_3\} \cup (N_{v_5}^{(0)} \Delta N_{v_3}^{(v_2)}). \end{aligned} \tag{17}$$

If m is odd, the neighborhoods evolve as

$$\begin{aligned} N_{v_{m-2}}^{(v_{m-1})} &= N_{v_{m-1}}^{(0)} \setminus \{v_{m-2}\}, \\ N_{v_m}^{(v_{m-1})} &= \{v_{m-2}\} \cup (N_{v_m}^{(0)} \Delta N_{v_{m-2}}^{(v_{m-3})}). \end{aligned} \quad (18)$$

After performing all measurements, both $v_1 = a_{i,j}$ and $N_{v_1=a_{i,j}}^{(0)}$ will be contained in $N_{v_m=r}^{(v_{m-1})}$, the final neighborhood of the root. The initial neighborhood of the root $N_{v_m=r}^{(0)} \setminus \{v_{m-1}\}$ will still be connected to the root.

If m is even, we can use the same procedure up to v_{m-1} . Then, without loss of generality, we choose party i from $\{i, j\}$ and perform an $X[v_{m-1}, i]$ measurement. After this measurement, we have neighborhoods

$$\begin{aligned} N_i^{(v_{m-1})} &= N_{v_{m-1}}^{(v_{m-2})} \setminus \{i\}, \\ N_{v_m}^{(v_{m-1})} &= \{i\} \cup (N_{v_m}^{(0)} \Delta N_i^{(0)}). \end{aligned} \quad (19)$$

The result is $N_{v_{m-1}}^{(v_{m-2})} \setminus \{i\}$, previously containing parties $\{i, j\}$, now being part of N_i , connecting j to i . Furthermore, i is now connected directly to $v_m = r$.

Finally, if the root is a party, the protocol is complete. If not, we X-measure the root and Z-measure all neighbors of parties which are not parties themselves, connecting and isolating the three chosen parties. □

C Measurement Counts

In this Appendix, we demonstrate compare the number of measurements needed to complete DODAG-X with the X-protocol.

Theorem 3 *The DODAG-X protocol and the X-protocol both require the same number of measurements for $n \leq 3$ parties when run on the same tree structure.*

To prove Theorem 3, we categorize all measurements into two groups: those taken along the path between nodes to entangle, and the isolating measurements performed at the end of the protocol. We compose a proof for three parties $\{i, j, k\}$, which applies equally to the case of two parties.

C.1 Path Measurements

In [18] the authors determine the total number of path measurements M by considering the paths P_{ij} and P_{jk} , giving

$$\begin{aligned} M &= |P_{ij} \cup (P_{jk} \setminus (P_{ij} \cap P_{jk}))| - n \\ &= |P_{ij} \cup P_{jk}| - n \end{aligned} \quad (20)$$

where the subtraction of n comes from excluding the measurements of the parties themselves. On the other hand, for the DODAG-X protocol, the total number of path measurements M' is

$$M' = |P_{i,r} \cup P_{j,r} \cup P_{k,r}| - n, \quad (21)$$

where $P_{i,r}$ is the path from party $i \in \{n\}$ to the root r . To show that $P_{ij} \cup P_{jk} = P_{i,r} \cup P_{j,r} \cup P_{k,r}$, we can write the paths from i to j , and from j to k , as

$$\begin{aligned} P_{ij} &= (P_{i,r} \cup P_{j,r}) \setminus (P_{i,r} \cap P_{j,r}) \cup a_1, \\ P_{jk} &= (P_{j,r} \cup P_{k,r}) \setminus (P_{j,r} \cap P_{k,r}) \cup a_2, \end{aligned} \quad (22)$$

where $a_1 = a_{i,j}$ and $a_2 = a_{j,k}$ are the intersections defined previously in Section 3, in a simplified notation. Using properties of the symmetric difference, we can rewrite

$$\begin{aligned} P_{ij} &= (P_{i,r} \setminus P_{j,r}) \cup (P_{j,r} \setminus P_{i,r}) \cup a_1, \\ P_{jk} &= (P_{j,r} \setminus P_{k,r}) \cup (P_{k,r} \setminus P_{j,r}) \cup a_2. \end{aligned} \quad (23)$$

Given a tree structure, we know that for all $j \neq i \in \{n\}$ we have

$$P_{i,r} \setminus P_{j,r} = P_{i,a_{i,j}} \setminus \{a_{i,j}\}. \quad (24)$$

Therefore, we can write paths P_{ij} and P_{jk} as

$$\begin{aligned} P_{ij} &= (P_{i,a_1} \setminus \{a_1\}) \cup (P_{j,a_1} \setminus \{a_1\}) \cup a_1, \\ &= P_{i,a_1} \cup P_{j,a_1}. \\ P_{jk} &= (P_{j,a_2} \setminus \{a_2\}) \cup (P_{k,a_2} \setminus \{a_2\}) \cup a_2, \\ &= P_{j,a_2} \cup P_{k,a_2}. \end{aligned} \quad (25)$$

Given Eq. (25) we have

$$P_{ij} \cup P_{jk} = (P_{i,a_1} \cup P_{j,a_1}) \cup (P_{j,a_2} \cup P_{k,a_2}). \quad (26)$$

We can rewrite the path from j to a_2 in the form $P_{j,a_2} = P_{j,a_1} \cup P_{a_1,a_2}$, giving

$$\begin{aligned} P_{ij} \cup P_{jk} &= P_{i,a_1} \cup P_{j,a_1} \cup P_{a_1,a_2} \cup P_{k,a_2}, \\ &= (P_{i,a_1} \cup P_{a_1,a_2}) \cup (P_{j,a_1} \cup P_{a_1,a_2}) \cup P_{k,a_2}, \\ &= P_{i,a_2} \cup P_{j,a_2} \cup P_{k,a_2} \end{aligned} \quad (27)$$

Since there are at most two intersections for any three parties, we can relabel a_2 as r without loss of generality. Therefore

$$P_{ij} \cup P_{jk} = P_{i,r} \cup P_{j,r} \cup P_{k,r}. \quad (28)$$

This proves the total number of measurements for both the DODAG-X and X-protocols over the path is the same for a tree structure. □

C.2 Isolation Measurements

In [19], the authors show that X measurements on the repeater line do not affect the overall neighborhood of the line, except for the vertices removed by measurement. The total number of isolating measurements is determined by the initial neighborhood of the path, minus the vertices removed during the protocol from measurement. For a tree, the nodes $N_{v_n} \cap N_{v_{n+2}} = \{v_{n+1}\}$ are the only nodes removed by X-measurement during the protocol when measuring v_{n+1} . The final isolation measurements are given by the total neighborhood, described by

$$N_T = \bigcup_{v \in P_{i,r} \cup P_{j,r} \cup P_{k,r}} N_v^{(0)}, \quad (29)$$

minus the nodes measured through the path union, defined previously as $P_{i,r} \cup P_{j,r} \cup P_{k,r}$. The same analysis applies for the X-protocol, and the total amount of measurements for both protocols can be written

$$|N_T| - |P_{i,r} \cup P_{j,r} \cup P_{k,r}| = |N_T| - |P_{ij} \cup P_{jk}|. \quad (30)$$

Therefore, by the analysis in Section C.1, both protocols require the same number of isolating measurements in a tree structure. □

D Additional Performance Benchmarks

This Appendix benchmarks the repeater protocol against the X-protocol [18]. The repeater protocol first isolates the shortest path between nodes using Z-measurements, then performs X-measurements along the path. The X-protocol does not isolate the path first. We give these plots to show the performance of both protocols on networks of different topologies, sizes, and configurations. Figure 14 gives this comparison for a grid.

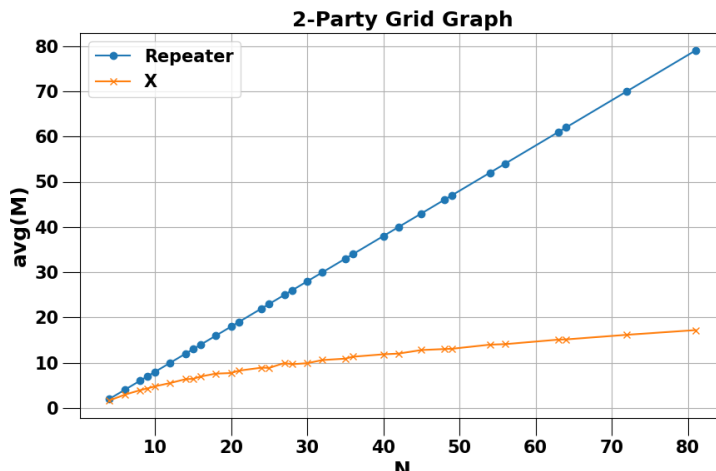


Figure 14: Average measurements to entangle two parties in a grid graph.

The X protocol requires fewer measurements compared to the repeater protocol, especially as the number of nodes increases. The average measurements for the X protocol grows logarithmically with N .

Figure 15 gives a performance comparison for star graphs and Small-World graphs. In star graph networks, both protocols require the same number of measurements. In Small-World graphs, the X protocol performs better, especially for larger networks. The performance also depends on the values of p and k .

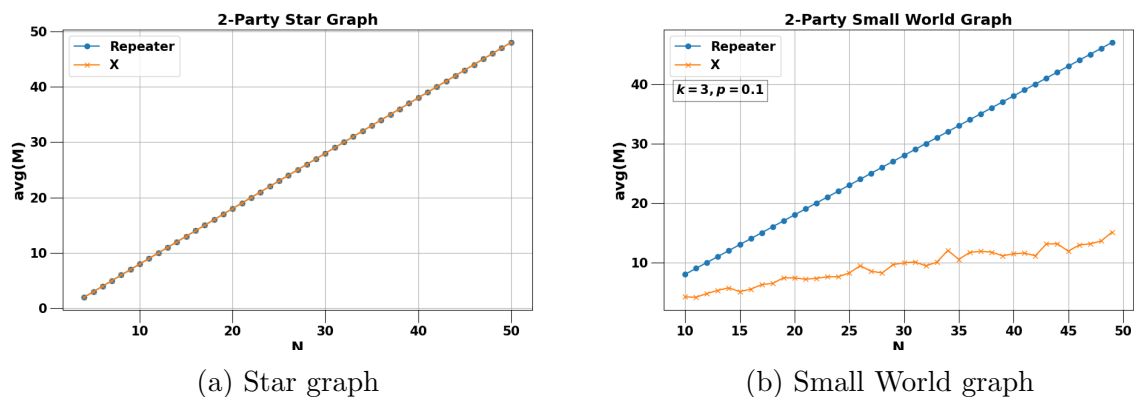
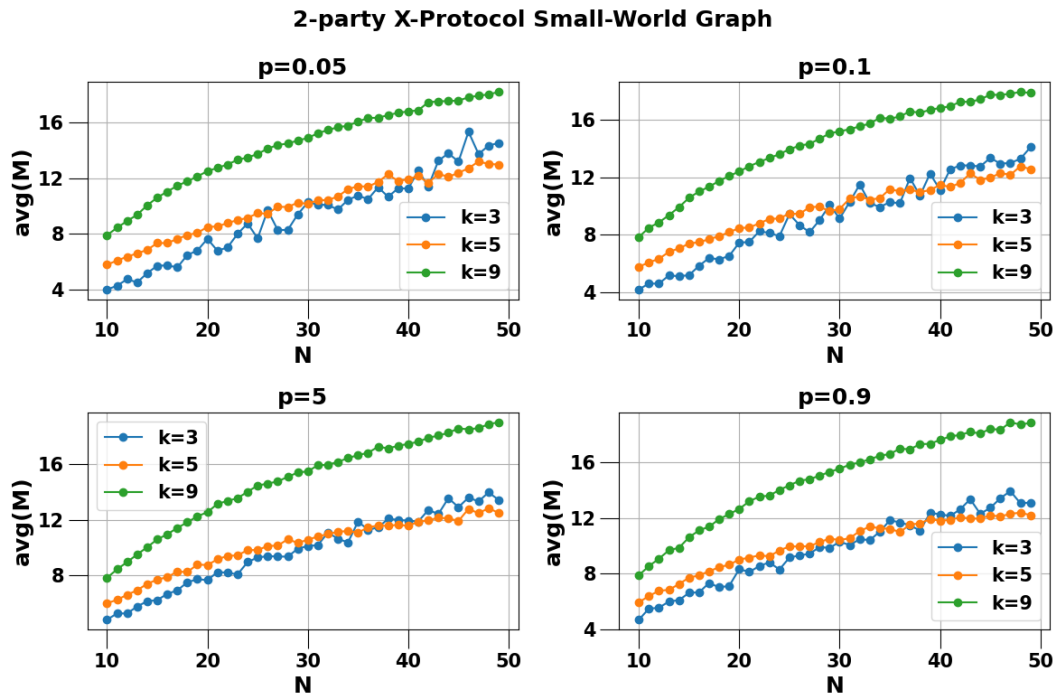
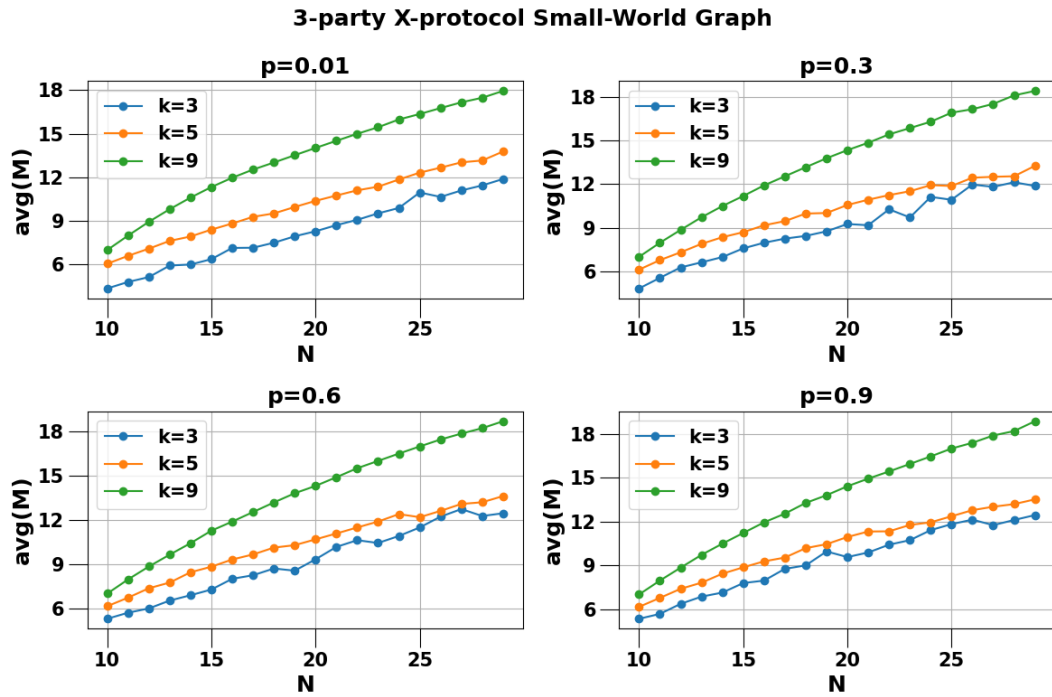


Figure 15: Average measurements in different network configurations.

Figure 16 shows X protocol performance for 2 and 3 parties in Small-World networks.



(a) 2-party protocol



(b) 3-party protocol

Figure 16: Average measurements in Small-World graphs for different combinations of p and k , for 2 and 3-party X-protocol.